Diffusion and Deformations of Single *Hydra* Cells in Cellular Aggregates

Jean Paul Rieu,* Arpita Upadhyaya,[†] James A. Glazier,[†] Noriyuki Bob Ouchi,[‡] and Yasuji Sawada[‡]

*Département de Physique des Matériaux, Université Claude Bernard, Lyon I, 69622 Villeurbanne Cedex, France; [†]Department of Physics, University of Notre Dame, Notre Dame Indiana 46556, USA; and [‡]Research Institute of Electrical Communication, Tohoku University, Aoba-ku, Sendai 980–77, Japan

ABSTRACT   Cell motion within cellular aggregates consists of both random and coherent components. We used confocal microscopy to study the center of mass displacements and deformations of single endodermal *Hydra* cells in two kinds of cellular aggregates, ectodermal and endodermal. We first carefully characterize the center of mass displacements using standard statistical analysis. In both aggregates, cells perform a persistent random walk, with the diffusion constant smaller in the more cohesive endodermal aggregate. We show that a simple parametric method is able to describe cell deformations and relate them to displacements. These deformations are random, with their amplitude and direction uncorrelated with the center of mass motion. Unlike for an isolated cell on a substrate, the random forces exerted by the surrounding cells predominate over the deformation of the cell itself, causing the displacements of a cell within an aggregate.

INTRODUCTION

Cell migration plays a central role in many biological processes. Coordinated movements in epithelial layers occur during morphogenesis in the embryo (Armstrong, 1985) and during wound healing (Clarck, 1996). In the inflammatory response or in metastasis, individual cells migrate into the circulatory system (Bray, 1992). Migration also helps patterns form, e.g., in cell-sorting and tissue regeneration (Trinkaus and Lentz, 1964; Gierer et al., 1972; Technau and Holstein, 1992; Mombach et al., 1995), tissue engulfment (Kishimoto et al., 1996), aggregation of amoebae (Loomis, 1995), and collective motion of bacteria (Budrene and Berg, 1995).

Extensive studies exist of cell locomotion by single cells on substrates coated with different adhesive molecules and for different buffers (for a recent reference, see Hinz et al., 1999). Reconstruction from time-lapse images over long times of center of mass trajectories has shown that cells perform a persistent random walk in the absence of chemotactic sources or cell-cell interactions (DiMilla et al., 1992; Lee et al., 1994; Czirok et al., 1998). The cell speed, the percentage of motile cells, and the persistence time all reach a maximum for intermediate levels of cell-substrate adhesiveness (DiMilla et al., 1993). At smaller length scales, single-cell locomotion depends on cell deformation and requires a complex series of mechanical and molecular processes such as membrane extension, attachment to the substrate, generation of force, and detachment from the substrate (Lauffenburger and Horwitz, 1996). Sophisticated microscopy, digital image processing, and computer-as-

sisted analysis (Killich et al., 1993; Schindl et al., 1995; Hinz et al., 1999) have now clarified these processes.

Within aggregates and tissues, cells directly contact other cells and do not move independently of one another. Both displacements and deformations may depend on individual cell properties (internal cytoskeletal dynamics, membrane elasticity) as well as tissue properties (cell-cell adhesion, correlations due to close packing in the aggregate). We expect two different behaviors depending on the adhesive properties of the tissues: cells may migrate either as coherent groups if adhesion is strong, or as individuals otherwise (Phillips and Steinberg, 1978). An illustration of this hypothesis occurs during normal embryogenesis (Trinkaus, 1973). The tightly adhering epithelial cells form cohesive sheets that envelop deep cells. On a substrate, the epithelial cells spread as continuous sheets, and locomotion results primarily from the activity of the marginal cells, whereas the submarginal cells, which have only limited adhesion to the substratum, are passively dragged (DiPasquale, 1975). When epithelial cells change their shape, the epithelial sheets may stretch, bend, fold, or invaginate (Odell et al., 1981). The loose deep cells migrate in an apparently random fashion when they are not densely packed (Fink and Trinkaus, 1988).

However, changes in relative epithelial cell position occur during gastrulation in *Fundulus*, epiboly in fish, and the morphogenesis of *Hydra* (Keller and Trinkaus, 1987; Bray, 1992). When multiple types of cells from a primitive animal or an embryo are dissociated, randomly intermingled, and then reaggregated, they are able to rearrange, to re-establish coherent homotypic domains, and sometimes to reconstitute an entire animal. This rearrangement of cells, known as cell sorting, requires individual cell movements (Mombach et al., 1995). In two-dimensional (2D) aggregates of dissociated endodermal and ectodermal *Hydra* cells, motion during sorting consists of both random and coherent components (Rieu et al., 1998). Coherent motion appears due to aggregate or internal endodermal cluster rounding; motion seems

---

random otherwise. The motion of single pigmented cells in 3D aggregates of chick embryonic neural cells is also random in the absence of sorting or rounding effects (Mombach and Glazier, 1996). *Dictyostelium* mounds before cell sorting exhibit self-organized coherent rotational motion in both 2D and 3D aggregates (Rietdorf et al., 1996). Later during cell sorting, random, linear, and rotational motions all appear in 3D aggregates (Doolittle et al., 1995).

We have previously noted that for single cells, motion is faster for intermediate cell-substrate adhesion (DiMilla et al., 1993). Within aggregates, a cell stops moving as an individual when adhesion is strong (DiPasquale, 1975). However, the role of intermediate cell-cell adhesion on individual cell mobility has been poorly investigated quantitatively. The only studies of this topic to our knowledge are the viscoelastic and interfacial measurements for chick cell aggregates (Forgacs et al., 1998). The relaxation time of compressed aggregates correlates with the tissue surface tension: the lower the surface tension, the faster the long time scale relaxation. Tissue surface tensions arise from the cohesive and adhesive interactions of their component cells (Foty et al., 1996). Lower surface tension indicates lower tissue cohesiveness (i.e., smaller cell-cell adhesion). Faster relaxation indicates higher cell mobility. Hence, cell mobility seems to anticorrelate directly with cell-cell adhesion.

During in vitro cell sorting, cells deform. Chick embryonic cells in the interior of confluent monolayers are able to ruffle and translocate relative to one another (Garrod and Steinberg, 1975). The inhibition of membrane activity by adding cytochalasin-B to the culture medium prevents large scale cell sorting in these embryos (Mombach et al., 1995). However, understanding the mechanisms of cell translocation requires detailed and quantitative studies of cell deformations in cellular aggregates. A parametric method successfully characterizes deformations, rotations, and displacements of single cells or cell populations and their correlations (Germain et al., 1999). This method seems difficult to apply to individual cell motion in cellular aggregates where all the component cells move together. However, we have retained this model's idea, reducing the cell dynamics to a small number of parameters.

Although a large body of work characterizes cell motion, none of it has studied quantitatively both cell motion and the corresponding changes in cell shape within densely packed cellular aggregates. Our primary motivation is to quantify the cell mobility in two types of cellular aggregates with different cohesiveness. Second, we want to characterize the dynamics of cell deformations within aggregates and to determine how they relate to cell displacements. We study simultaneously center of mass displacements and cell deformations in 2D aggregates of dissociated *Hydra* cells. We observe by confocal microscopy the motion of autofluorescent endodermal cells in two kinds of cellular aggregates with different cohesiveness: pure endodermal or ectodermal aggregates. Here, the endodermal aggregates are the more

cohesive (Sato-Maeda et al., 1994; Rieu et al., 1998). In order to compare cell mobility in different cellular aggregates, we first check carefully that the endodermal cell displacements are random. We also examine the parameters required by the large-Q Potts model simulations to account for the experimental results. We then characterize cell shape changes and, finally, study their correlation with cell center of mass displacements.

MATERIALS AND METHODS

Strain and culture

Hydra viridissima shows good contrast between unstained endodermal and ectodermal cells due to the presence of symbiotic algae inside endodermal cells (Campbell, 1973; Rieu et al., 1998). We cultured *Hydra* supplied by Dr. H. Shimizu (National Institute of Genetics, Mishima, Japan) at 18°C in Loomis' solution (Gierer et al., 1972), fed them 4 times a week with freshly hatched *Artemia nauplii* shrimp, and transferred them to fresh culture solution 5 h after feeding. We starved the animals for 24 to 36 h before experiments.

Preparation of dissociated cell aggregates

Mechanical dissociation and reaggregation of *hydra* cells in dissociation medium (DM) at 4°C followed the method of Gierer et al. (1972). After removing the heads and feet from a group of 3 to 5 animals, we separated the ectodermal and endodermal layers using procaine-HCl (Wako Pure Chemicals, Tokyo, Japan) according to the method of Kishimoto et al. (1996). We minced the tissues separately and almost completely dissociated them into single cells by gentle shearing by repeated pipetting. We held the cell preparation (5–8 ml) for 30 min in DM at 4°C to sediment and sheared it again. We then filtered it using a 53-μm nylon mesh (NRK, Tokyo, Japan) and centrifuged it at $250 \times g$ for 5 min to sediment and collect the epithelial cells. We observed the motion of the unstained endodermal cells in two cellular environments, pure endodermal aggregates (A) and ectodermal aggregates (B). For case A, we used endodermal cell pellets; for case B, we added a small percentage of endodermal cells (~10%) to the ectodermal cell preparation before centrifugation.

Microscopy

We cut the pellets into fragments about 1 mm in diameter and placed them between cover glasses with 25-μm width spacers to form essentially 2D aggregates (Rieu et al., 1998). The cover glasses were clamped together and placed in a petri dish containing dissociation medium and observed with a two-channel confocal microscope (Olympus IX70-KrAr-SPI, Japan). For the fluorescence channel, we used light of 568 nm. Comparison of transmission and fluorescence images of a single endodermal cell on a solid substrate (Fig. 1, *a* and *b*) shows that the autofluorescent symbiotic algae uniformly fill the cytoplasm, but are absent near the membrane. Such images reveal large amplitude cell shape changes but not the ruffling and pseudopodal activity of the membranes occurring at smaller scales. In transmission the (nonfluorescent) ectodermal cells (Fig. 1 *c*) appear lighter than the endodermal cells (Fig. 1 *a*). Within aggregates, cells pack densely and their contours become indistinguishable in transmission at 20× magnification (Fig. 1 *d*). About 50% of the endodermal cells autofluoresce. We can, therefore, find regions of pure endodermal aggregates containing isolated fluorescent cells. Cell displacements and deformations in time-lapse images are clearly visible at 1-min time intervals (see, for instance, the two cells marked by arrowheads in Fig. 1 *e*). These movements appear random to the eye. By watching larger areas of the sample over longer
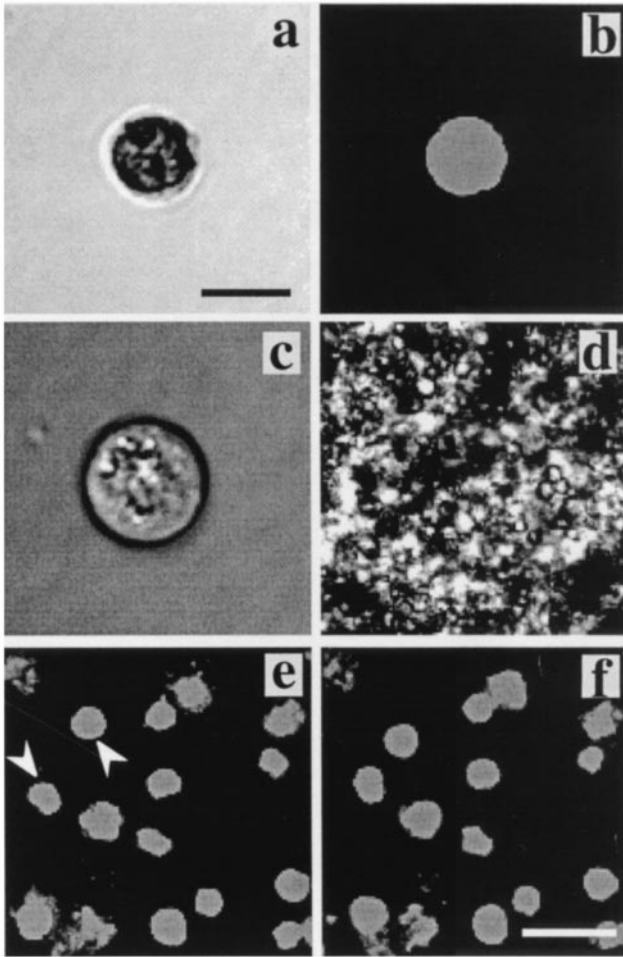
FIGURE 1 Confocal images of *Hydra* cells. A single endodermal cell on a solid substrate observed (*a*) by optical transmission and (*b*) by fluorescence; (*c*) a single ectodermal cell observed by optical transmission; an endodermal aggregate observed (*d*) in optical transmission and (*e*) in fluorescence (arrowheads indicate two cells that move closer together); (*f*) the same aggregate 3 min later. Bars, 10 μm (*a-c*) and 25 μm (*d–f*).

times, we often observed collective motion in some parts of the aggregate. Collective behavior may provide some interesting information on the tissue cell properties, but at the same time it depends strongly on the sample geometry, making interpretation difficult (Rieu et al., 1998). Our motivation here is to study quantitatively changes in cell mobility in different cellular aggregates; thus, we present only those experiments without collective behavior.

Image processing

We recorded the 2D motion of several sets of cells for cases A and B, with each set containing 15 to 30 cells in the field of view. Image intervals were $\Delta t = 30$ s (1 min in some cases) during 40 to 80 min with an Olympus 20× objective lens (10× in some cases). We digitized images directly using dedicated software. At 512 × 512 pixels, the resolution was about 0.15 μm/pix, which suffices to track center of mass motion and to characterize large scale cell deformations for cells of 10 μm diameter. We analyzed the images using NIH-Image software (a public domain program available at http://rsb.info.nih.gov/nih-image) to obtain the time series for the center of

mass of each cell using our own tracking program (Rieu et al., 1998). We used the x_i and y_i coordinates (or the vector position $\vec{r}_i$) of the center of mass of each cell i to study cell displacements and their relevant statistics. To analyze the cell shape changes, we saved images from NIH-Image as text files of intensity images and used our own FORTRAN and MATLAB programs to calculate cell contours and other statistics. From the intensity profile, we extracted the cell contour as follows: we chose the intensity threshold to be the point at which the profile had maximum slope. We obtained the cell contour by binary thresholding, defining intensity values above the threshold as outside the cell and values below the threshold as within the cell.

Measurement of motion parameters

For a 2D persistent random walker, $\langle \rho^2 \rangle$, the mean squared displacement (MSD), and $C(t)$, the velocity autocorrelation function, are functions of time t, diffusion constant D, persistence time t_p, and cell speed S (Dunn, 1983):

$$\langle \rho^2(t) \rangle = 4D(t - t_p(1 - e^{-t/t_p})), \qquad (1)$$

$$C(t) = S^2 e^{-t/t_p}. \qquad (2)$$

For $t \ll t_p$, $\langle \rho^2 \rangle$ is parabolic with time, whereas for $t \gg t_p$, $\langle \rho^2 \rangle$ becomes linearly dependent on t, which is the signature of normal diffusion. The three parameters are related as $D = \frac{1}{2}S^2 t_p$ (Dickinson and Tranquillo, 1993). For a set of cells tracked during $t_{max} = N\Delta t$, we can calculate the MSD as a function of the time interval t:

$$\langle \rho^2(t) \rangle = \langle (x_i(t_0 + t) - x_i(t_0))^2 + (y_i(t_0 + t) - y_i(t_0))^2 \rangle, \quad (3)$$

where we take the average over all cells in a set (typically 15) and over all possible t_0 using overlapping intervals (Dickinson and Tranquillo, 1993). We use the instantaneous velocity of the cell i at time t, $\vec{v}_i(t) = (\vec{r}_i(t + \Delta t) - \vec{r}_i(t))/\Delta t$ to calculate the autocorrelation function of the velocity $C(t) = Z(t)/Z(0)$ with $Z(t) = \langle \vec{v}_i(t_0 + t) \cdot \vec{v}_i(t_0) \rangle$. We determined values of D, t_p, and S by fitting Eqs. 1 and 2 to experimental data for time intervals less than $t_{max}/3$. Over longer times, insufficient intervals are available for averaging, and the error in the fitted parameters may increase dramatically (Dunn, 1983; Dickinson and Tranquillo, 1993).

Characterization of cell deformations

In the images, most cells are quasi-spheres (see Fig. 1, *e* and *f*, and Fig. 7). We neglected a few cells whose mean shape was nonspherical. Our quantitative characterization of cell deformations follows the method of Germain et al. (1999). We calculate the amplitude (ϕ) and direction (θ) of maximum and minimum cell deformation between two successive time intervals. We define these quantities as follows. (1) We calculate the cell radius $d_j(t)$ at every 2° angular increment through the center of mass (angle of each radius d_j with the horizontal, $\theta_j = j \times 2°$). (2) We calculate the amplitude of deformation after $\Delta t = 30$ s along the direction j as $\phi_j(t) = d_j(t + \Delta t) - d_j(t)$. (3) At each time t, we keep as working parameters the maximum and minimum of $\phi(t)$ and their corresponding orientations, $\phi_{max}(t)$, $\phi_{min}(t)$, $\theta_{max}(t)$, and $\theta_{min}(t)$. $\phi_{max}(t)$ and $\phi_{min}(t)$ correspond to the cell extension amplitude and the cell contraction amplitude, respectively.

We calculate the correlations of the cell deformations following a method used to study fluctuating vesicles (Schneider et al., 1984) and membrane fluctuations of the erythrocyte membranes (Brochard and Lennon, 1975). We can describe the fluctuating shape in terms of a displacement vector of a membrane element from its position on the original sphere to its position on the deformed sphere. The radial component of the displacement represents the local curvature of the quasi-sphere, which we expand in a set of normal modes. The first mode, $m = 0$, represents expansion and contraction of the cell radius, which is negligible due to the

constant area and volume of the cell. The $m = 1$ mode represents the center of mass displacement of the cell. The $m = 2$ mode represents the long wavelength fluctuations (ellipsoidal deformations) of the cell membrane, which we analyze. From the cell contour images, we measure the difference between two perpendicular diameters $e = l(\theta) - l(\theta + \pi/2)$. The time correlation function of the cell deformations is $R(t) = \langle e(t_o + t) \times e(t) \rangle$, where the average is over 18 diameters i every 10° and over t_o.

Potts model simulations of cell motion

The extended large-Q Potts model, first introduced by Graner and Glazier (1992), uses a spin σ_{ij} at each lattice site, (i, j). A given cell is defined by the set of all sites with the same spin σ. Each cell has an associated cell type τ. The energy per unit surface area depends on cell type, $J_{\tau\tau'}$. We introduce three cell types, $\tau \in \{l, d, m\}$, where l is for ectodermal cells, d is for endodermal cells, and m is for the culture medium. In 2D simulations, we introduce the cell size as a target area A_τ and a target perimeter l_τ. The latter modifies previous simulations (Graner and Glazier, 1992) in order to prevent the splitting of cells into many subcells in the case of negative surface energies J. Thus, the total energy is

$$H = \sum_{(ij)-(i'j')} J_{\tau\tau'}(1 - \delta_{\sigma,\sigma'}) + \left\{ \lambda_1 \sum_\sigma (a(\sigma) - A_\tau)^2 \right.$$

$$\left. + \lambda_2 \sum_\sigma (l(\sigma) - l_\tau)^2 \right\}(1 - \delta_{\tau,m}), \quad (4)$$

where $a(\sigma)$ and $l(\sigma)$ are, respectively, the area and perimeter of cell σ, and λ_1 and λ_2 are the elasticity parameters. At each step, we apply the Metropolis method and accept a proposed change in spin value at a site with a transition probability dependent on temperature $T > 0$, $p = \{exp(-\Delta H/T):\Delta H > 0; 1:\Delta H \leq 0\}$.

We choose the surface energies to satisfy the sorting condition, i.e., $J_{dm} > J_{dl} + J_{lm} - J_{ll}$ and $J_{ll} - J_{dd} \approx J_{dd} - J_{ld}$, and we choose the other parameters to ensure complete sorting in the simulation. We use a square lattice of 128×128 sites where the initial state is a circular aggregate with about 300 cells. We investigate two kinds of aggregates (with 100% d cells or with <5% d cells) and two kinds of surface energies. We first use the same positive surface energies as in previous simulations ($T = 10$, $J_{ll} = 14$, $J_{dd} = 2$, $J_{dl} = 11$, $J_{dm} = J_{lm} = 16$, $A_l = A_d = 20$, $\lambda_1 = 10$, and $\lambda_2 = 0$). We then use negative surface energies ($T = 10$, $J_{ll} = -5$, $J_{dd} = -25$, $J_{ld} = -3$, $J_{lm} = 1$, $J_{dm} = 20$, $\lambda_1 = 10$, $A_l = A_d = 20$, $\lambda_2 = 5.5$, and $l_l = l_d = 22$).

We compute for each case the MSD and other statistics of d cells for each configuration, using Eq. 3 and averaging the results over 16 cells.

RESULTS

Experimental observations

Fig. 2 shows the center of mass trajectories of a set of endodermal cells in endodermal aggregate no. 1 at 30-s intervals over 39 min. Trajectories are characteristic of persistent random motion: sudden turns disrupt approximately linear movements 5 to 10 μm in length, lasting 3 to 5 min. Periods of small random fluctuations without any significant center of mass displacement and without persistence often occur between two persistent periods (trapped motion). Endodermal cells in an ectodermal aggregate show similar trajectories, but with larger displacements and less trapped motion.
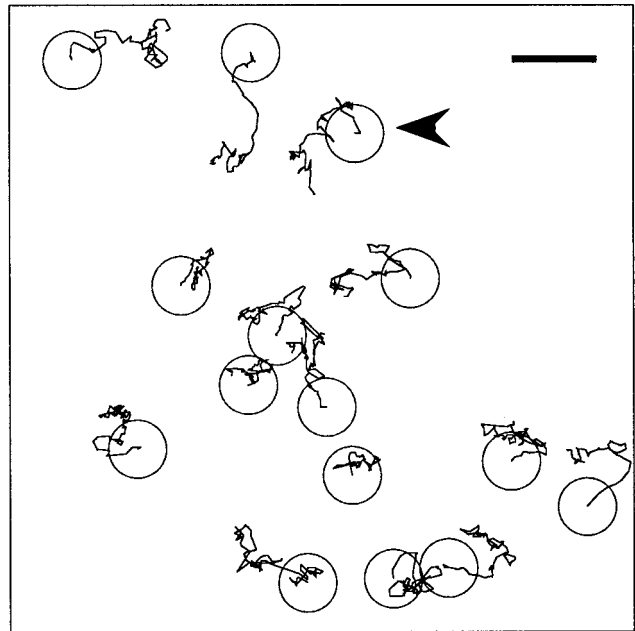
FIGURE 2 Trajectories of 15 endodermal *Hydra* cells in endodermal aggregate no. 1 over 39 min. Dots indicate center of mass positions at 30-s intervals. Big circles show the approximate cell size and the initial cell position. An arrowhead signals a cell whose trajectory and shape is studied in detail in Fig. 8. Bar, 10 μm.

Characterization of center of mass displacements

In an isotropic environment, cells move as persistent random walkers. As previously stated, when drift or cellular flows superimpose on diffusion in our experiment, the MSD $\langle \rho^2 \rangle$ is no longer linear in time (Upadhyaya A., J. P. Rieu, J. A. Glazier, and Y. Sawada, manuscript submitted to *Physica A*). For the present experiments, we first plot $\langle \rho^2 \rangle$ as a function of time interval (Fig. 3). The behavior seems linear but, as the trajectories last only a finite experimental time, our statistics could overlook anomalous diffusion (Bouchaud and Georges, 1990). The central limit theorem provides more precise characterization of any kind of diffusion process. It states that the diffusion is anomalous whenever one of the following two conditions fails:

1. The distribution $P(X_t)$ of the position $X_t = x_i(t_0 + t) - x_i(t_0)$ is not too broad (for instance, a power-law distribution $P(X_t) \sim X_t^{-\beta}$ with $\beta \geq 3$) and takes, at large time scales, t, a Gaussian form.

2. No long-range correlations exist, i.e., the autocorrelation function $C(t)$ decays more rapidly than t^{-1}.

The first condition does not hold for the so-called Levy flight distributions. A persistent random walker satisfies both. In particular, the autocorrelation function decays exponentially (Eq. 2). The review of Bouchaud and Georges (1990) and references therein give a more rigorous discussion of random walks and central limit theorem.
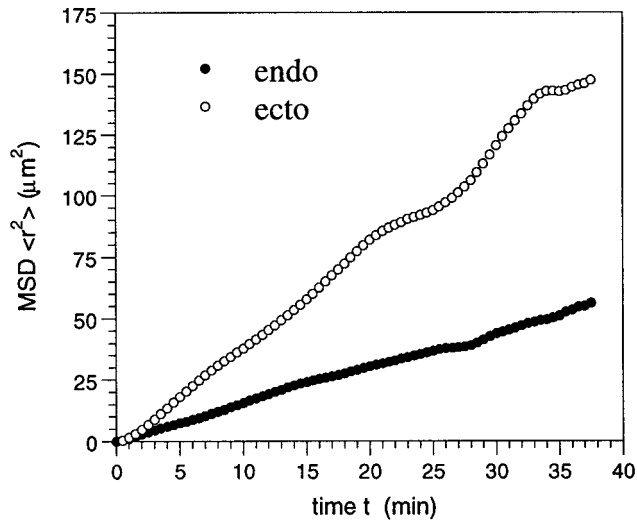
FIGURE 3 Mean squared displacements (MSD) averaged along the trajectory as a function of interval time (Eq. 3) for endodermal cells in endodermal aggregate no. 1 (*bullets*), and endodermal cells in ectodermal aggregate no. 3. (*circles*). Both curves are reasonably linear at large times indicating normal diffusion, and parabolic at short times indicating persistent movement. Table 1 reports the parameters obtained from the fit of the averaged MSD using standard analysis (Eq. 1).

We present in Fig. 4 the probability distribution for the cells of Fig. 2 for $t = 30$ s and $t = 3$ min. The centers of both distributions differ only slightly from $X_t = 0$, indicating almost no collective drift of these cells. For $t = 30$ s, which is the time step size, a Gaussian fits the tail of our experimental distribution poorly (Fig. 4 *A*, solid line). The agreement is much better with the form proposed by Tsallis and Buckman (1996), which has an asymptotic power-law behavior $P(X_t) \sim X_t^{-\beta}$ for large X (dashed line), with an exponent $\beta = 4$. The distribution is therefore not too broad ($\beta > 3$) and should converge toward a Gaussian for large time scales, t. Indeed, we find that our data fit a Gaussian for $t = 3$ min (Fig. 4 *B*), indicating that cell motion becomes diffusive at this time scale. For smaller time scales, either persistent or trapped motions dominate. For ectodermal aggregates, the distributions are qualitatively the same, but a little broader for $t = 30$ s and much broader for $t = 3$ min. This broadening corresponds to the larger MSD in ectodermal aggregates at large times.

The velocity autocorrelation function $C(t)$ as a function of time interval t sheds light on the short-time persistent behavior. When flows or collective drift are present, $C(t)$ exhibits a long tail, which roughly fits a decaying power law $t^{-\beta}$ with $\beta < 1$ (Upadhyaya, A., J. P. Rieu, J. A. Glazier, and Y. Sawada, manuscript submitted). Elsewhere, the autocorrelation function decreases rapidly to zero (Fig. 5 *A*). At long times, velocities are uncorrelated ($C(t) = 0$), consistent with a persistent random walk. Using a power law fit, we find $\beta > 1$, indicating clearly the absence of long range correlations in the experiments we present. However, a decaying exponential (Eq.
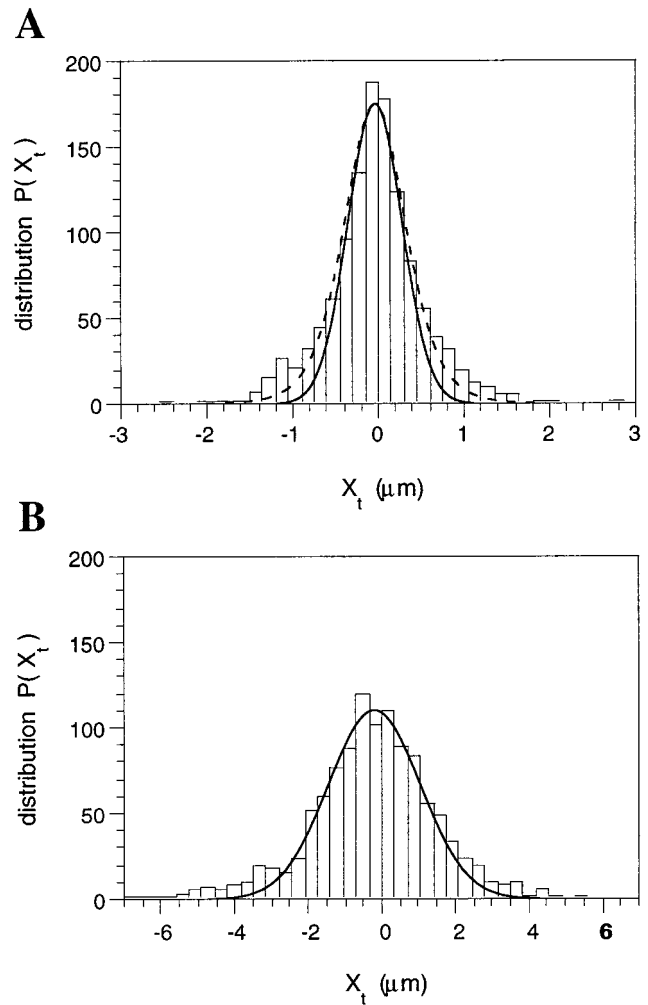

FIGURE 4 Distributions $P(X_t)$ of the cell positions $X_t = x_i(t_0 + t) - x_i(t_0)$ along the *x* axis for endodermal cells in endodermal aggregate no. 1 during time intervals of *t*. (*A*) For $t = 30$ s, the form proposed by Tsallis and Buckman (1996), which has an asymptotic power-law behavior $P(X_t) \sim X_t^{-\beta}$ for large X (*dashed line*) fits the experimental distribution better than the Gaussian (*solid line*). (*B*) At $t = 3$ min, the agreement with the Gaussian (*solid line*) is satisfactory.

2) fits the data much better (Fig. 5 *A*). Table 1 reports the values of the fitted parameters. Below, we discuss in detail our estimates for the persistence time and cell speed.

As we are now confident that the presented experiments show normal diffusion, we can return to our analysis of the MSD plots using the standard analysis for persistent random walks (Eq. 1). This analysis satisfactorily accounts for the MSD in both aggregates. Table 1 gives the fitting parameters for these experiments. The most striking result is that the diffusion constant is always smaller in endodermal aggregates. Averaging over 2 experiments for each type of aggregate, we obtain $D_{ecto} = 1.05 \pm 0.4$ $\mu m^2/min$ and $D_{endo} = 0.45 \pm 0.2$ $\mu m^2/min$. The limited number of runs prevented us from measuring the dependence of persistence
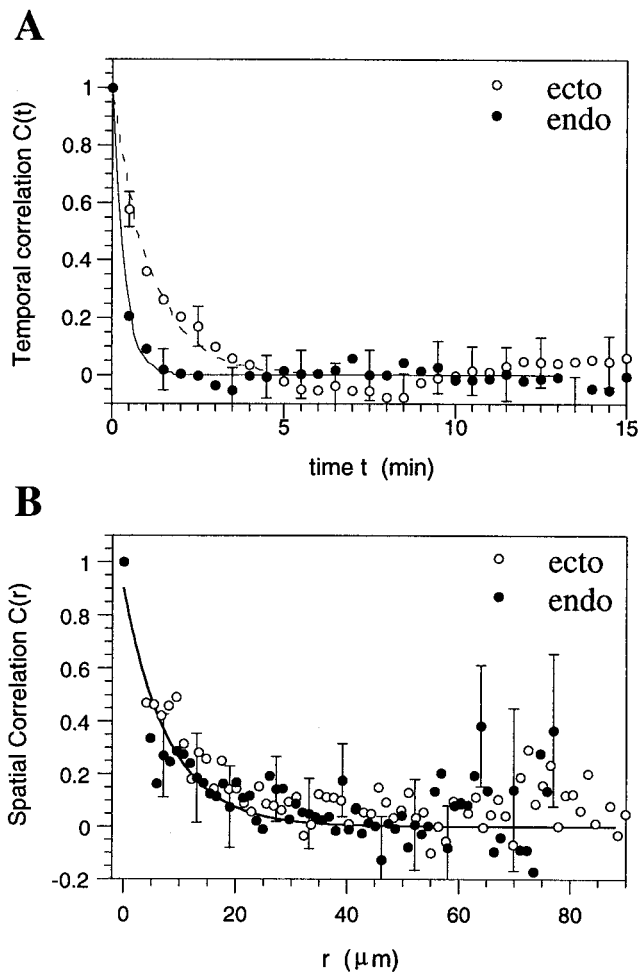
A

B

FIGURE 5   (*A*) Autocorrelation function of the velocity as a function of the time interval *t* for endodermal cells in endodermal aggregate no. 1 (*bullets*), and endodermal cells in ectodermal aggregate no. 3 (*circles*). Fits with an exponential function are also displayed for endodermal (*solid line*) and ectodermal aggregates (*dashed line*). Table 1 reports the values of the fitted parameters. (*B*) Spatial correlation of the cell velocity (see text) in endodermal aggregate no. 1 (*bullets*) and in ectodermal aggregate no. 3 (*circles*). The solid line is a fit of the endodermal aggregate with an exponential.

time on aggregate type. However, the values of the persistence time obtained from the MSD (t_{p1}) and from the autocorrelation function of the velocity (t_{p2}) are similar. Also, values of cell speed *S* obtained from the autocorrelation function are close to the ones deduced from the relation $S = \sqrt{2D/t_p}$. The analysis is fully self-consistent.

However, we may slightly underestimate the absolute values of the parameters *D* and t_p because we also include the trapped cells in our analysis using the persistent random walk model. In their analysis of the motion of isolated human tissue cells, DiMilla et al. (1992) excluded immotile cells, which exhibit negligible displacements over long observation times. In our case, their criteria seem difficult to adopt because most of our cells sometimes stop, rest, and

then move again. The distribution $P(\theta)$ of angles between successive displacements offers an alternative method to evaluate the persistence time. We define these displacements during a time interval *t* as $\vec{\delta r}_t(t_0) = \vec{r}(t_0 + t) - \vec{r}(t_0)$. For short times, the distribution presents a continuum background with an excess of small angles corresponding to correlated cells (Fig. 6 *A* for endodermal aggregate no. 1). In ectodermal aggregate no. 3 (Fig. 6 *B*), the background is smaller and the small angles dominate. An excess of small angles persists for up to 3 to 5 min in both types of aggregate. For longer times, the distribution is flat; the orientations of successive displacements are uncorrelated; the cells execute a pure random walk. We define the proportion of correlated cells as $P_C = (N_T - 2N_{90})/N_T$ where N_T is the total number of angles and N_{90} the number of angles larger than 90°. $2N_{90}$ represents, crudely, the number of angles within the background. This quantity, plotted as a function of time interval (Fig. 6 *C*), shows correlations at larger times than the autocorrelation function (Fig. 5 *A*). By fitting the curves to an exponential for times less than $t_{max}/3$, we find correlation times $t_{p3} = 2.4$ and 3.5 min instead of 0.4 and 1 min, respectively, for ectodermal and endodermal aggregates nos. 3 and 1. Table 1 gives the values of t_{p3} together with $P_C(1)$, the proportion of cells remaining correlated at 1-min intervals. The proportion of correlated cells seems larger in ectodermal aggregates. The difference in the values of t_p given by each method results from the presence of trapped cells, which introduce noise in the statistics at small time scales in standard analysis and which disappear at longer times. Whatever the method, the value of the persistence time is very low for living cells (Fink and Trinkaus, 1988; DiMilla et al., 1992).

Finally, we calculate the spatial correlations of the velocity, $C(r) = Z(r)/Z(0)$ with $Z(r) = \langle \vec{v}(r_i) \times \vec{v}(r_j) \rangle$, as a function of the distance between cells $r = r_i - r_j$. The average is over all cells of the same type and over all times analyzed. This quantity decreases to zero and remains zero indicating uncorrelated velocities at large distances (Fig. 5 *B*). The same behavior occurs for both types of aggregate. The data fit an exponential, and we find a correlation length of approximately 12 μm in both experiments, corresponding to one cell diameter (i.e., the displacements of first neighbors correlate), which is not surprising because the cells are in close contact.

Cell shape changes

Fig. 7 plots the contours at 1-min intervals of an endodermal cell within ectodermal aggregate no. 3. The overall shape changes slowly and deviates just slightly from a sphere at each time. Small bumps called blebs (Trinkaus, 1973) appear frequently (see the arrowheads at $t = 6$ min and $t = 9$ min in Fig. 7). The bleb on the bottom right at $t = 9$ min seems to spread as a lamellipodium at the next time, $t = 10$ min. However, such thick protrusions are rare. The cell

TABLE 1   Values of the model parameters discussed in the text

	Endo aggregate		Ecto aggregate	
	No. 1	No. 2	No. 3	No. 4
N_{Cells}	15	15	17	13
D (μm^2/min)	0.40 ± 0.04	0.55 ± 0.08	1.0 ± 0.10	1.1 ± 0.07
t_{p1} (min)	0.28 ± 0.15	1.0 ± 0.40	0.65 ± 0.35	1.05 ± 0.50
$\sqrt{2D/t_{p1}}$ (μm/min)	1.69 ± 1.1	1.05 ± 0.6	1.75 ± 1.1	1.44 ± 0.8
S (μm/min)	1.45 ± 0.04	1.10 ± 0.03	1.43 ± 0.04	1.57 ± 0.04
t_{p2} (min)	0.35 ± 0.2	1.0 ± 0.4	1.1 ± 0.4	0.8 ± 0.4
t_{p3} (min)	2.4 ± 0.7	3.1 ± 1.0	3.5 ± 0.7	6.3 ± 1.5
$P_c(1)$ (%)	20 ± 7	46 ± 10	51 ± 10	40 ± 10

contours are always very smooth and do not present filipodia or ruffles. Some cells do not change their shape during long periods of time, even when they move long distances (Fig. 8 A).

In order to characterize these deformations, we first study the time series of cell expansion and contraction amplitudes and directions for two different aggregates. Fig. 8 shows the results for the cell marked with an arrowhead in Fig. 2 (endodermal aggregate no. 1), and Fig. 9 is for the cell already displayed in Fig. 7 (ectodermal aggregate no. 3). On average, the expansion and contraction amplitudes ϕ_{max} and ϕ_{min} are symmetrical with similar amplitudes (Figs. 8 B and 9 B), indicating that the cell area is roughly constant during the analysis, as expected. More interesting are the estimates of mean amplitude deformations in the two kinds of cellular aggregates. On average, over 5 cells in both cases, we obtained $\langle\phi_{max}\rangle_{endo} = 0.29$ μm in endodermal aggregates and $\langle\phi_{max}\rangle_{ecto} = 0.45$ μm in ectodermal aggregates. The amplitude of deformation is higher in ectodermal aggregates. Fig. 10 A presents the histogram of $\theta_{max} - \theta_{min}$ for the cell of Fig. 8. This angle is the difference between directions of extension (θ_{max}) and contraction (θ_{min}). The distribution lies mainly between 30° and 110°, indicating different kinds of deformations. Unexpectedly, the maximum of the distribution is not at 90° (ellipsoidal deformations), but rather at 60°. These deformations seem to correspond to the appearance of blebs in the cell contours of Fig. 7.

Fig. 11 shows the time correlations of the ellipsoidal cell deformations $R(t)$ (see Materials and Methods) in endodermal aggregate (average of over 5 cells). We find that the time correlation of cell membrane fluctuation is exponential, decaying as $A exp - t/\tau$ for both aggregates, where A and τ are, respectively, the mean squared amplitude and correlation time of the deformations. This decay indicates that deformations are essentially uncorrelated beyond a characteristic time τ. We find $A_{ecto} = 0.55 \pm 0.25$ μm^2, $\tau_{ecto} = 3.2 \pm 2$ min for the endo-ecto case and $A_{endo} = 0.35 \pm 0.20$ μm^2, $\tau_{endo} = 5.1 \pm 2$ min for the endo-endo case (values averaged over 5 cells in both cases). Interestingly, the correlation time for the deformations is approximately the same as the persistence time of the center of

mass motion. Though, for the sake of simplicity, we only study ellipsoidal deformations, the results are qualitatively the same for other kinds of deformations.

Since we have characterized cell deformations by a few parameters, we ask whether we can identify these modes of the correlations as determining features of cell migration, as Germain et al. (1999) found percentages with a similar parameterization for single fibroblasts on a solid substrate. Figs. 8 B and 9 B present the simultaneous time series of the amplitudes of the center of mass displacement (solid line). In endodermal aggregate no. 1, this displacement is always larger or equal to ϕ_{max}. It shows large fluctuations, whereas the deformations are rather uniform. Deformations and displacements are only equal during the time interval $t = 6$ to $t = 10$ min. This period corresponds to the trapping period (Fig. 8 A). When motion becomes persistent ($t = 10$ to $t = 16$ min), displacements are large but not deformations (see ϕ_{max} in Fig. 8 B or simply the cell contours at times 10, 13, and 16 min in Fig. 8 A). In ectodermal aggregates, the amplitudes of displacements and deformations seem uncorrelated as well, but they are generally of the same magnitude (Fig. 9 B). Between $t = 7$ and $t = 10$ min, the cell has moved slightly to the bottom right, and the cell shape changes due to the spreading of a lamellipodium (see arrowheads in the bottom of Fig. 7). Between $t = 10$ and $t = 13$ min, the center of mass has moved toward the bottom, and the shape elongates in this direction (Fig. 9 A). This figure suggests at least transient correlations between cell deformation and cell displacement in ectodermal aggregates. In order to learn more about the properties of these correlations, we plotted the histogram of $\theta_{max} - \theta_{disp}$ where θ_{disp} corresponds to the direction of displacement. The distribution is approximately flat (Fig. 10 B). The small variations around the mean are within the statistical error. We obtained similar histograms for $\theta_{min} - \theta_{disp}$, θ_{max}, θ_{min} and θ_{disp} for each type of aggregate. The flatness of the three last histograms means that deformations and displacements have no preferred direction. We conclude that the directions of cell deformation and cell displacement are mainly uncorrelated. We also studied cross-correlations between θ_{disp} at time t_o and θ_{max} or θ_{min} at time $t_o + t$. Again, we did not find any evidence of correlation.
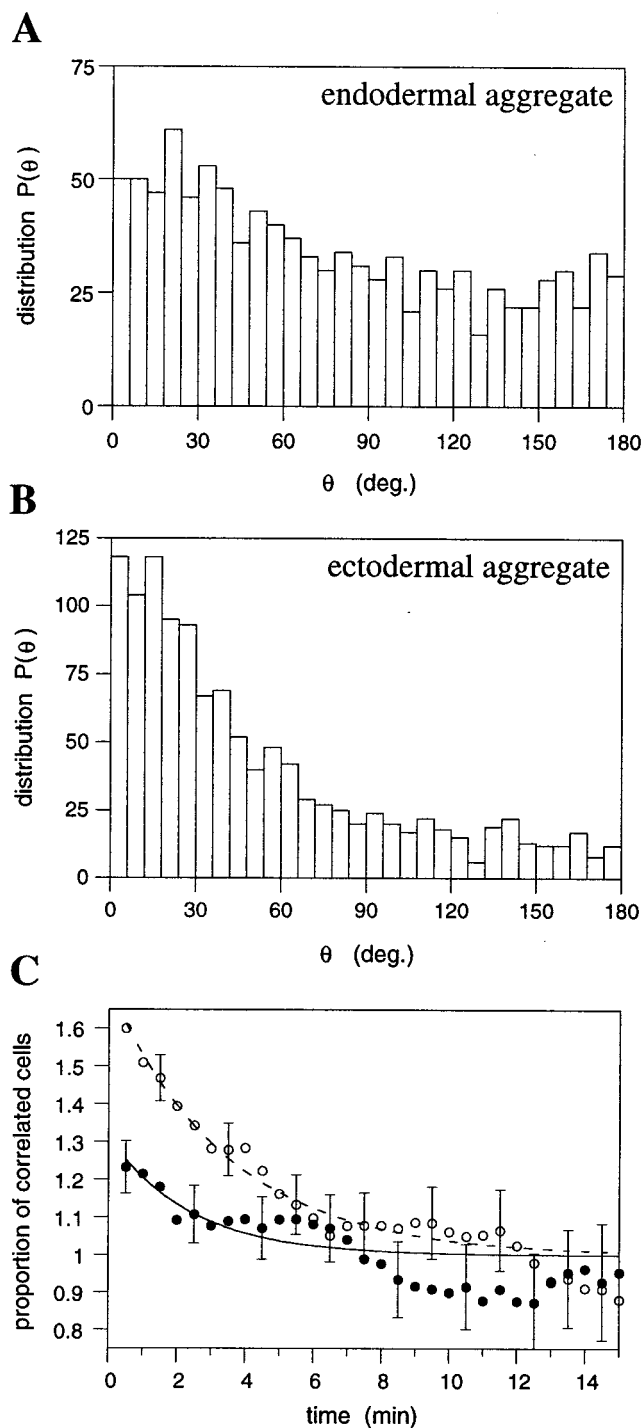
A

B

C

FIGURE 6 (*A*) Distributions of angles between successive displacements (see text) during time intervals $t = 30$ s for (*A*) endodermal aggregate no. 1 and (*B*) ectodermal aggregate no. 3. (*C*) Proportion of correlated cells as a function of the time interval, *t*, (see text) for ectodermal (*bullets*) and endodermal aggregates (*circles*). Fits with an exponential function are also displayed for endodermal (*solid line*) and ectodermal aggregates (*dashed line*). Table 1 reports values of the fitted parameters.
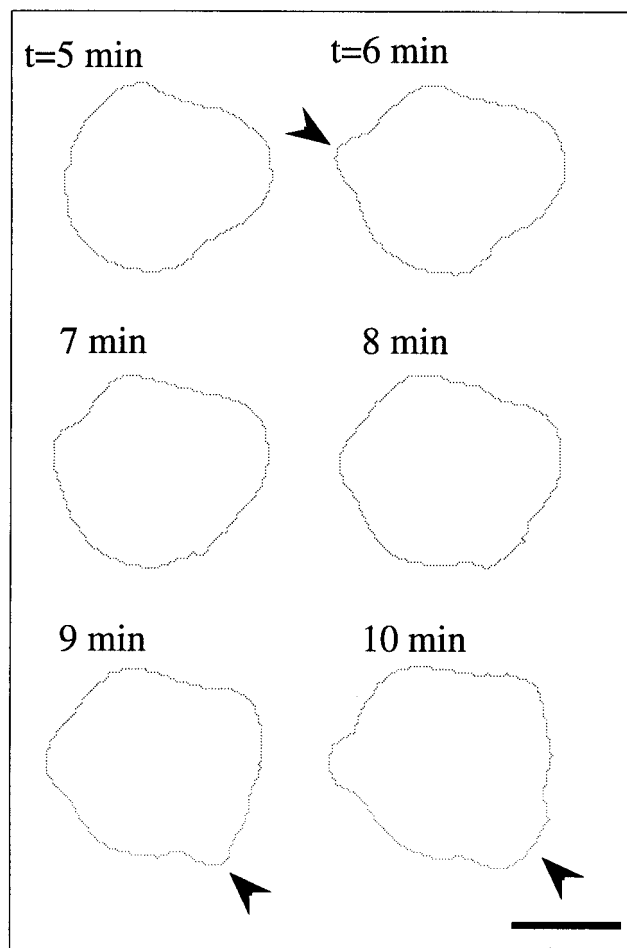
FIGURE 7 Contours of a cell within an ectodermal aggregate every 1 min (see numbers). Arrowheads at $t = 6$ min and $t = 9$ min show blebs on the contours. The bleb at $t = 10$ min is thicker and resembles a lamellipodium. Bar, 5 μm.

DISCUSSION

Using the autofluorescent *Hydra viridissima* and a 2D experimental geometry, we have been able to perform detailed observations and analyses of individual cell displacements and cell deformations within densely packed cellular aggregates. The voluminous work of Trinkaus et al. on the motion of deep cells throughout the subepithelial space of the yolk sac during embryogenesis (Trinkaus, 1973; Fink and Trinkaus, 1988; Trinkaus et al., 1992; and other references therein) is, to our knowledge, the only other detailed study of this type. However, the previous authors observed regions where the cells clustered loosely. Because both individual and collective movement of cells play a role during embryogenesis and cancer metastasis (Grimstad, 1987), our results and methods are very important: they show directly for the first time that within aggregates, (i) cell may move not by their own deformations but because of external
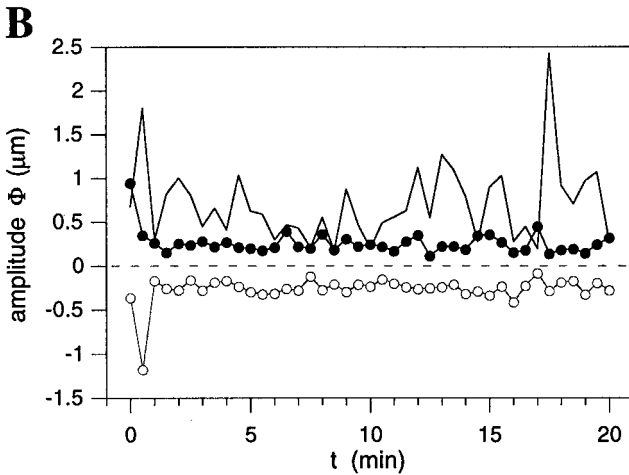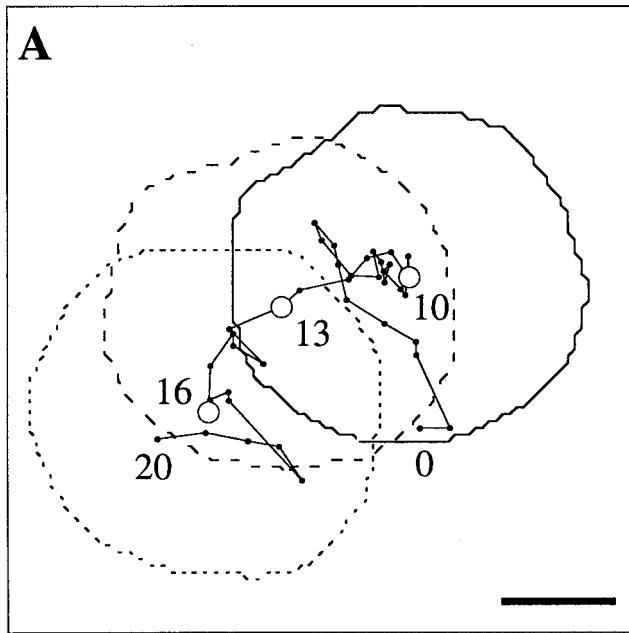
FIGURE 8   (*A*) Contours of a cell within endodermal aggregate no. 1 at *t* = 10, 13 and 16 min respectively from right to left. Large circles represent the center of mass at these times. Dots represent the rest of the center of mass trajectory over 20 min and at 30-s intervals. Numbers indicate times. (*B*) Time series of the cell extension amplitude ϕ_{max} (*bullets*), the cell contraction amplitude ϕ_{min} (*circles*), and the center of mass displacements (*solid line*) during 30 s (see text) for the same cell.

FIGURE 9   (*A*) Contours of a cell within ectodermal aggregate no. 3 at *t* = 7, 10, and 13 min, respectively, from the top to the bottom (same cell as in Fig. 7). Large circles represent the center of mass at these times. *Dots* represent the rest of the center of mass trajectory over 13 min at 30-s intervals; numbers indicate times (7 is the beginning of the trajectory). (*B*) Time series of the cell extension amplitude ϕ_{max} (*bullets*), the cell contraction amplitude ϕ_{min} (*circles*), and the center of mass displacements (*solid line*) during 30 s (see text) for the same cell.

fluctuations, and (ii) motion is faster in less cohesive aggregates, e.g., in ectodermal aggregates.

Cell shape changes do not primarily induce center of mass displacement

The endodermal cell shapes changes resemble the hemispherical protrusions, called blebs, that make deep cells advance in the direction of their leading edge (Trinkaus, 1973). We sometimes observed transient correlations be-
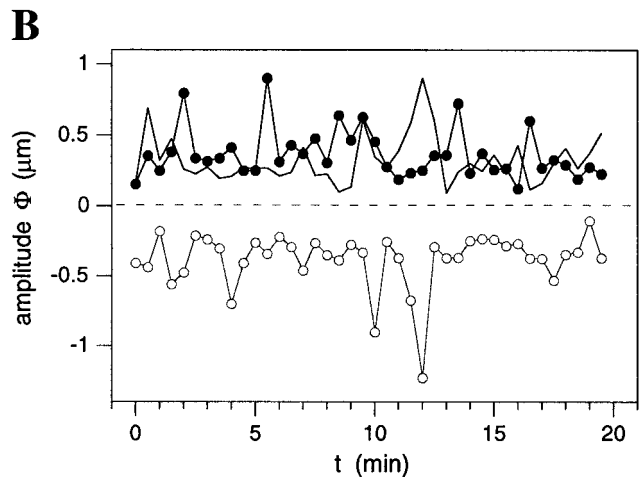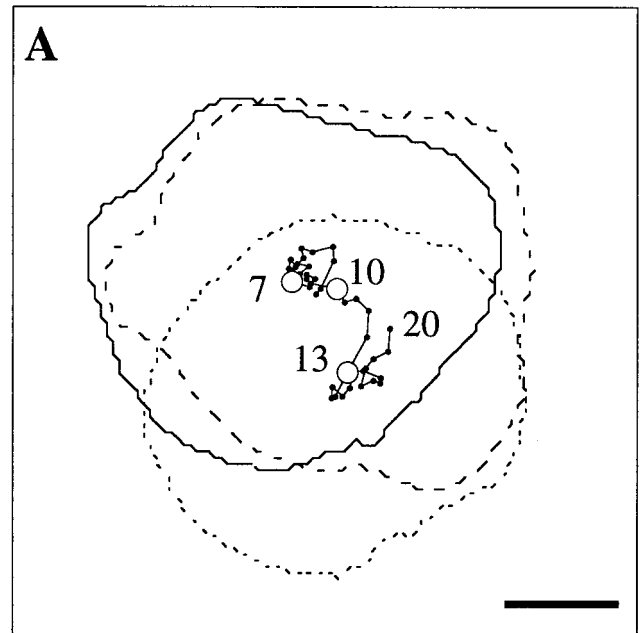
tween these deformations and the direction of center of mass translocation in ectodermal aggregates. However, statistically, the direction and amplitude of cell deformation do not correlate with the direction and amplitude of cell displacement for the 10 cells studied in detail here. We often observe large center of mass displacements without simultaneous cell deformations (Fig. 8 *A*). The mean amplitude of deformation is often smaller than the displacement amplitude. Thus, unlike deep cells or isolated cells on a substrate,
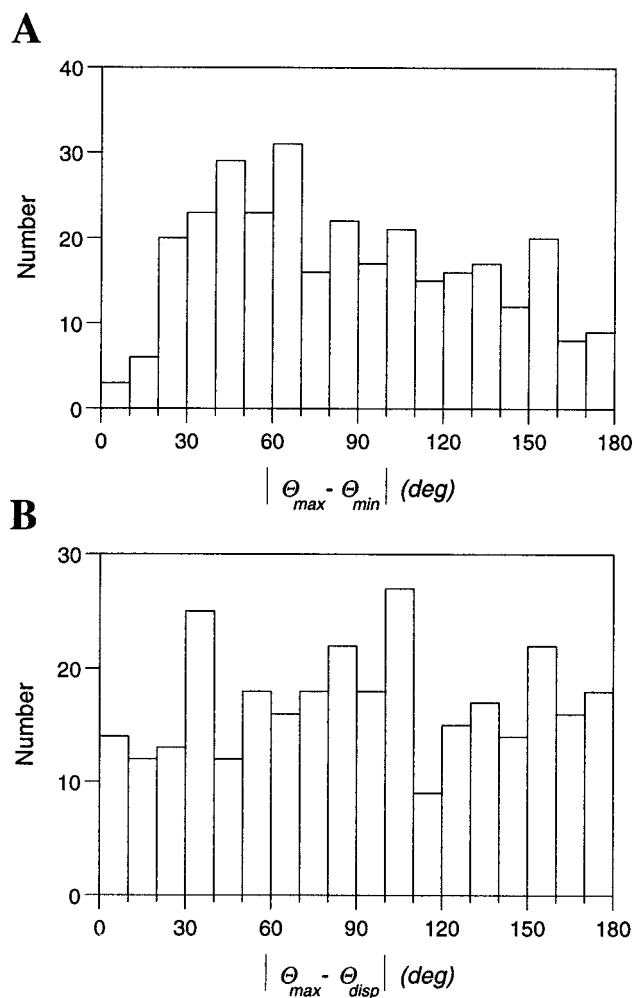
A

B

FIGURE 10 (*A*) Distributions of the difference between directions of extension and contraction. (*B*) Distributions of the difference between directions of extension and center of mass displacement. The two distributions were obtained from 5 cells in endodermal aggregates.

FIGURE 11 Time correlation of the cell deformations, $R(t) = \langle e_i(t_o + t)e_i(t_o)\rangle$ as a function of time interval (see Materials and Methods) in endodermal aggregates (averaged over 5 analyzed cells).

endodermal cells within aggregates move not only by their own deformations, but because of the external forces exerted by the deformations of the neighboring cells. The situation in a sense is similar to Brownian motion. A Brownian particle moves randomly because liquid molecules kick it. Here, the cell receives continuous shoves from other cells with a characteristic persistence time. The difference between the two cases is that the liquid molecules have uncorrelated fluctuations and no shear modulus, whereas in our case, the surrounding consists of strongly interacting (and even sticking) deformable units (the cells).

Effective temperature and effective viscosity of cellular aggregates

Due to the above mentioned difference between liquid and cellular baths, the Stoke's law for viscous drag f on a
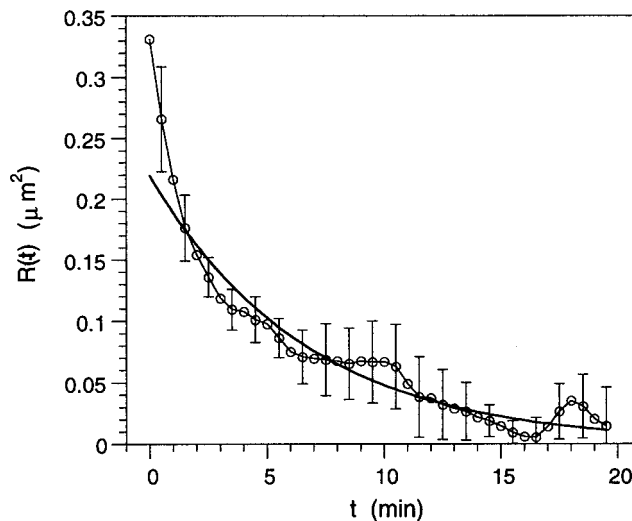
Brownian particle of radius R moving at speed v in a viscous fluid of viscosity η, $f = -6\pi\eta Rv$ (Reif, 1985) certainly fails for tissues, as does the corresponding equation for the diffusion constant of Brownian particles, $D = k_B T/6\pi\eta R$. However, the comparison with Brownian motion illuminates the physical parameters governing cell motion. For tissues, T is, of course, an effective temperature. $k_B T$ is the fluctuation energy arising from cell activity (actin polymerization dynamics) and from the energy released during bond formation. The viscous dissipation arises from the energy required to rupture bonds and to deform the cells (membrane rigidity and cytoplasmic viscosity). We expect the viscous dissipation to be larger in the more cohesive tissue because it costs more energy to break bonds. Forgacs et al. (1998) have experimentally verified, using chicken embryonic tissues, that more cohesive tissues are more viscous. We expect the same will hold for *Hydra*. In our experiments, the diffusion is at least two times smaller in the more cohesive endodermal aggregates. A difference in fluctuation energy of the cellular bath could also contribute to the observed difference in diffusion constant, as indicated by the study of the correlations of cell deformations. Despite the complexity of the underlying processes, the deformations relax on a single time scale, as observed for vesicles fluctuating in a viscous medium. For those vesicles, the correlation time measures of the effective viscosity of the cellular aggregate and the amplitude represents effective temperature (Schneider et al., 1984). Here, the amplitude of endodermal deformation is higher while the correlation time is smaller in ectodermal aggregates, indicating that effective temperature is higher while effective viscosity is smaller in ectodermal aggregates. In ectodermal aggregates, cells sometimes appear to move more autonomously (Fig. 9 *A*)

with an apparently higher degree of directional persistence (Fig. 6 *C*).

Simulations of cell motion

Previous Potts model simulations showed that the simulation temperature controls the cell deformations and the cell mobility (Mombach et al., 1995). Here, we examine the role of both temperature and surface energy on the diffusion constant of simulated endodermal cells in homogeneous and rounded aggregates with different cohesivities. The results of the simulations will be published elsewhere in detail (N. B. Ouchi, J. A. Glazier, J. P. Rieu, A. Upadhyaya, and Y. Sawada, manuscript in preparation). Briefly, we first find, as expected, that in homogeneous aggregates the diffusion constant increases with increasing temperature if all the other parameters are constant. At constant temperature and with positive surface energies, decreasing the surface energies, that is, increasing the cohesivity, enhances the diffusion constant. This increase results from the higher probability to deform (increase cell perimeter) in the case of lower surface energy (i.e., simulated endodermal aggregates). For the opposite hierarchy, we need to use negative surface energies in the Potts simulation. These results support our hypothesis that different surface energies with a uniform simulation temperature playing the role of the membrane fluctuations suffice to model differences in cell mobility within an aggregate. These simulated parameters seem more relevant to describe the behavior of cells within aggregates than the effective temperature and effective viscosity introduced in the comparison with Brownian motion. However, simulations do not show directional persistence of their locomotion, nor collective behaviors at larger times as found in experiments. We can easily introduce persistent motion in the Potts model by adding a term to the Hamiltonian constraining the instantaneous velocity to be its previous velocity (A. Upadhyaya and J. A. Glazier, manuscript in preparation).

Persistence and correlations at short times

Most cell motion results from pressure from the moving masses of other cells. However, *Hydra* cells do not maintain the same neighbors for long periods, as do submarginal cells of epithelial layers on a substrate (DiPasquale, 1975). The spatial correlation of the velocity indicates that only first neighbors correlate (Fig. 5 *B*). Cell-cell distance is never constant over time (see the two cells with arrowheads in Fig. 1 *e*); otherwise, it would prevent cell sorting of randomly intermixed *Hydra* cells. We sometimes clearly observe intercalation of a cell between others in transmission images. Even if we cannot exclude other mechanisms, we think the persistent portions of the cell trajectories between two trapped regimes (Fig. 9 *A*) correspond to intercalation, for

either a single cell or a group of cells (in this case, causing a larger rearrangement). Such rearrangements may be major cellular mechanisms dissipating tissue distortions caused by morphogenesis (Keller and Trinkaus, 1987). Here, we can reasonably assume that intercalation can also accommodate mechanical stresses in some parts of the aggregates. How can intercalation happen? Each cell can fluctuate a little, but as it binds to its nearest neighbors, these fluctuations generally produce a center of mass displacement not larger than some fraction of the cell diameter (trapped regime). When the pressure exerted by the neighbors becomes important in some direction, the cell has a finite chance to escape from its initial configuration. Escape can happen when simultaneous deformations of neighboring cells all push in a coordinated direction and reach a threshold. Fig. 12 shows two possibilities for such changes of configuration. For both, we have drawn initial, intermediate, and final configurations. The intermediate situation costs both contact area between cells (and thus the number of adhesive bonds) and local density. Once a local reorganization deviates sufficiently from the initial configuration, the next favorable configuration is the final one. Between them, the central cell has moved by roughly half a diameter in Fig. 12 *A* and by one diameter in Fig. 12 *B*. This motion is likely to be directed (persistent regime). A lower threshold in ectodermal aggregates due to lower cohesiveness might then explain the apparent higher directional persistence in ectodermal aggregates. Such a process is likely to happen for larger length scales (e.g., between cell clusters) and may explain the frequent appearance of collective motion at large times (J. P. Rieu and Y. Sawada, manuscript in preparation). We believe that the relevant parameters driving cell motion within aggregates are (i) the energy barriers associated with bond rupture and formation and (ii) packing constraints. We are currently trying to model cell motion within aggregates, taking into account these parameters and investigating the mechanisms which lead to coherent motion.
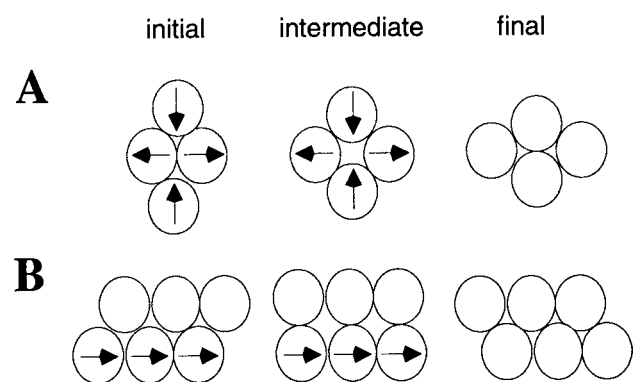

FIGURE 12 Two possible mechanisms of local configuration change: T1 process (*A*) and sliding of cell layers (*B*).

REFERENCES

Armstrong, P. B. 1985. The control of cell mobility during embryogenesis. *Cancer Metast. Rev.* 4:59–80.

Bouchaud, J-P., and A. Georges. 1990. Anomalous diffusion in disordered media: statistical mechanisms, models and physical applications. *Phys. Rep.* 195:127–293.

Bray, D. 1992. Cell Movements. Garland, New York and London.

Brochard, F., and J. F. Lennon. 1975. Frequency spectrum of the flicker phenomenon in erythrocytes. *J. Physique.* 36:1035–1047.

Budrene, E. O., and H. C. Berg. 1995. Dynamics of formation of symmetrical patterns by chemotactic bacteria. *Nature.* 376:49–53.

Campbell, R. D. 1973. Vital marking of single cells in developing tissues: India ink injection to trace tissue movements in hydra. *J. Cell Sci.* 13:651–661.

Clarck, R. A. F. 1996. The Molecular and Cellular Biology of Wound Repair, 2nd ed. Plenum, New York.

Czirok, A., K. Schlett, E. Madarász, and T. Vicsek. 1998. Exponential distribution of locomotion activity in cell culture. *Phys. Rev. Lett.* 81:3038–3041.

Dickinson, R. B., and R. T. Tranquillo. 1993. Optimal estimation of cell movement indices from the statistical analysis of cell tracking data. *Am. Inst. Chem. Eng. J.* 39:1995–2010.

DiMilla, P. A., J. A. Quinn, S. M. Albeda, and D. A. Lauffenburger. 1992. Measurements of individual cell migration parameters for human tissue cell. *Am. Inst. Chem. Eng. J.* 38:1092–1104.

DiMilla, P. A., J. A. Stone, J. A. Quinn, S. M. Albeda, and D. A. Lauffenburger. 1993. Maximal migration of human smooth muscle cells on fibronectin and type IV collagen occurs at an intermediate attachment strength. *J. Cell Biol.* 122:729–737.

DiPasquale, A. 1975. Locomotory activity of epithelial cells in culture. *Exp. Cell Res.* 94:191–215.

Doolittle, K. W., I. Reddy, and J. G. McNally. 1995. 3D Analysis of cell movements during normal and myosin-II-null cell morphogenesis in *Dictyostelium*. *Dev. Biol.* 167:118–129.

Dunn, G. A. 1983. Characterizing a kinesis response: time-averaged measures of cell speed and directional persistence. *Agents Actions Suppl.* 12:14–33.

Fink, R. D., and J. P. Trinkaus. 1988. Fundulus deep cells: directional migration in response to epithelial wounding. *Dev. Biol.* 129:179–90.

Forgacs, G., R. A. Foty, Y. Shafrir, and M. S. Steinberg. 1998. Viscoelastic properties of living embryonic tissues: a quantitative study. *Biophys. J.* 74:2227–2234.

Foty, R. A., C. M. Pfleger, G. Forgacs, and M. S. Steinberg. 1996. Surface tensions of embryonic tissues predict their envelopment behavior. *Development.* 122:1611–1620.

Garrod, D. R., and M. S. Steinberg. 1975. Cell locomotion within a contact-inhibited monolayer of chick embryonic liver parenchyma cells. *J. Cell Sci.* 18:405–425.

Germain, F., A. Doisy, X. Ronot, and P. Tracqui. 1999. Characterization of cell deformation and migration using a parametric estimation of image motion. *IEEE Trans. Biomed. Eng.* 46:584–600.

Gierer, A., S. Berking, H. Bode, C. N. David, K. Flick, G. Hansmann, H. Schaller, and E. Trenkner. 1972. Regeneration of *Hydra* from reaggregated cells. *Nat. New Biol.* 239:98–101.

Graner, F., and J. A. Glazier. 1992. Simulation of biological cell sorting using a two-dimensional extended Potts model. *Phys. Rev. Lett.* 69:2013–2016.

Grimstad, I. A. 1987. Direct evidence that cancer cell locomotion contributes importantly to invasion. *Exp. Cell Res.* 173:515–523.

Hinz, B., W. Alt, C. Johnen, V. Herzog, and H. W. Kaiser. 1999. Quantifying lamella dynamics of cultured cells by SACED, a new computer-assisted motion analysis. *Exp. Cell Res.* 251:234–243.

Keller, R. E., and J. P. Trinkaus. 1987. Rearrangement of enveloping layer cells without disruption of the epithelial permeability barrier as a factor in *Fundulus* epiboly. *Dev. Biol.* 120:12–24.

Killich, T., P. J. Plath, X. Wei, H. Bultmann, L. Rensing, and M. G. Vicker. 1993. The locomotion, shape and pseudopodial dynamics of unstimulated *Dictyostelium* cells are not random. *J. Cell Sci.* 106:1005–1013.

Kishimoto, Y., M. Murate, and T. Sugiyama. 1996. Hydra regeneration from recombined ectodermal and endodermal tissue. *J. Cell Sci.* 109:763–772.

Lauffenburger, D. A., and A. F. Horwitz. 1996. Cell migration: a physically integrated process. *Cell.* 84:359–369.

Lee, Y., L. V. McIntire, and K. Zygourakis. 1994. Analysis of endothelial cell locomotion: differential effects of motility and contact inhibition. *Biotechnol. Bioeng.* 43:622–634.

Loomis, W. F. 1995. Lateral inhibition and pattern formation in *Dictyostelium*. *Curr. Top. Dev. Biol.* 28:1–46.

Mombach, J. C., J. A. Glazier, R. C. Raphael, and M. Zajac. 1995. Quantitative comparison between differential adhesion models and cell sorting in the presence and absence of fluctuations. *Phys. Rev. Lett.* 75:2244–2247.

Mombach, J. C. M., and J. A. Glazier. 1996. Single cell motion in aggregates of embryonic cells. *Phys. Rev. Lett.* 76:3032–3035.

Odell, G. M., G. Oster, P. Alberch, and B. Burnside. 1981. The mechanical basis of morphogenesis. I. Epithelial folding and invagination. *Dev. Biol.* 85:446–462.

Phillips, H. M., and M. S. Steinberg. 1978. Embryonic tissues as elastico-viscous liquids: I. Rapid and Slow shape changes in centrifuged cell aggregates. *J. Cell Sci.* 30:1–20.

Reif, F. 1985. Fundamental of Statistical and Thermal Physics, international ed. McGraw-Hill, New York.

Rietdorf, J., F. Siegert, and C. J. Weijer. 1996. Analysis of optical density wave propagation and cell movement during mound formation in *Dictyostelium discoideum*. *Dev. Biol.* 177:427.

Rieu, J. P., N. Kataoka, and Y. Sawada. 1998. Quantitative analysis of cell motion during sorting in 2D aggregates of dissociated hydra cells. *Phys. Rev. E.* 57:924–931.

Sato-Maeda, M., M. Uchida, F. Graner, and H. Tashiro. 1994. Quantitative evaluation of tissue-specific cell adhesion at the level of a single cell pair. *Dev. Biol.* 162:77–84.

Schindl, M., E. Wallraff, B. Deubzer, W. Witke, G. Gerish, and E. Sackmann. 1995. Cell-substrate interactions and locomotion of *Dictyostelium* wild-type and mutants defective in three cytoskeletal proteins: a study using quantitative reflection interference contrast microscopy. *Biophys. J.* 68:1177–1190.

Schneider, M. B., J. T. Jenkins, and W. W. Webb. 1984. Thermal fluctuations of large quasi-spherical bimolecular phospholipid vesicles. *J. Physique.* 45:1457–1472.

Technau, U., and T. Holstein. 1992. Cell sorting during the regeneration of *Hydra* from reaggregated cells. *Dev. Biol.* 151:117–127.

Trinkaus, J. P., and J. P. Lentz. 1964. Direct observation of type-specific segregation in mixed cell aggregates. *Dev. Biol.* 9:115–136.

Trinkaus, J. P. 1973. Surface activity and locomotion of *Fundulus* deep cells during blastula and gastrula stages. *Dev. Biol.* 30:69–103.

Trinkaus, J. P., M. Trinkaus, and R. D. Fink. 1992. On the convergent cell movements of gastrulation in *Fundulus*. *J. Exp. Zool.* 261:40–61.

Tsallis, C., and D. J. Buckman. 1996. Anomalous diffusion in the presence of external forces: Exact time-dependent solutions and their thermostatistical basis. *Phys. Rev. E.* 54:R2197–R2200.